KSCE Journal of Civil Engineering (2018) 22(12):5026-5034
DOI 10.1007/s12205-017-1236-z

Structural Engineering
pISSN 1226-7988, eISSN 1976-3808
www.springer.com/12205

Research on Arch Effect and CFRP Strengthening Effect of RC Beams with Corroded Stirrups

Shuang Chen*, Haibo Lyu, Lei Wang***, and Xin Zhang******

Received August 24, 2017/Revised May 10, 2018/Accepted June 15, 2018/Published Online October 25, 2018

Abstract

In many cases the corrosion of steel reinforcement is considered to be the main reason that leads to the deterioration of the bond between steel reinforcement and concrete and causes the failure of members. However, stirrups with smaller diameter are more likely to get rusted and it is more difficult to find corrosion expansion cracks on the surface of concrete. Then the function of stirrups to restrict longitudinal bar from slipping will be weakened, which alters the mechanical properties and failure mode of corroded Reinforced Concrete (RC) beams. In this paper, the influence of corrosion of stirrups and the effect of strengthening corroded RC beams with Carbon Fiber Reinforced Polymer (CFRP) sheets were studied. The corrosion rate for each group varied between 0% to 18% which represented mass loss of the longitudinal steel reinforcement on the tension side. The longitudinal reinforcement of beams in Group A was not wrapped by the stirrups in order to simulate the situation that the stirrups were seriously corroded and lost their function. Beams of Group B were corroded control beams. Beams of Group C were corroded and then repaired by applying longitudinal CFRP sheets at the bottom and additional U-shaped CFRP sheets around the cross-section. Test results showed that the corrosion of stirrups had a detrimental effect on strength as well as the bond stress between steel bars and concrete. The mechanical mode of experimental beams tended to act like an arch. The greater the corrosion rate was, the more obvious the arch effect was. In addition, combining longitudinal and U-shaped CFRP sheets enhanced the ultimate load by an average of 56.5% of corroded RC beams. However, because of the longitudinal cracks, the strengthening effect of CFRP was much diminished when the corrosion rate was particularly high.

Keywords: *arch effect, stirrup failure, RC beam, strengthening, CFRP sheets*

1. Introduction

More and more reinforced concrete structures in harsh environment have experienced capacity or durability failure due to the corrosion of steel reinforcement, such as the buildings located nearby the coast or the bridges on which deicing salt is used in winter. For example, according to a recent report, corrosion exists in 89% of Reinforcement Concrete (RC) beams or plates of coastal buildings which have serviced for 7 to 25 years in China (Zeng, 2014). Corrosion causes the decrease of capacity of RC beams for three main reasons (Al-Hammoud *et al*., 2010; Al-Saidy *et al*., 2010; Coronelli and Gambarova, 2004;.Wang *et al*., 2016; Xue *et al.*, 2014): the loss in the effective cross-section area of rebar, the decrease of yield strength of rebar and the reduction of bond stress between the rebar and concrete. Furthermore, the surrounding concrete may crack or peel off due to the tensile stress caused by the expansion of corrosion products of the steel bars. The stirrup corrosion has also attracted the attention of scholars (Xia *et al*., 2011; Zhou *et al*., 2015). They realized that stirrups are relatively vulnerable to marine environment corrosion, as their protective layer is thinner. Although the stirrup confinement would increase bond performance of reinforcing steel in concrete, little is known regarding the effects of stirrup corrosion.

Since the late 80's, many universities, research institutions and manufacturers have carried out a large number of researches and applications in the use of Carbon Fiber Reinforced Polymer (CFRP) to reinforce or repair concrete structure around the globe (Badawi and Soudki, 2010; Kreit *et al*., 2014; Schnerch *et al*., 2006; Soudki and Sherwood, 2003). Based on those researches a lot of industry standards and specifications have been established in many countries. Compared with traditional strengthening methods, such as steel plate bonding, the advantages of using Fiber Reinforced Polymer (FRP) materials for retrofitting are: FRP is light in weight, have a high tensile strength, posses a high resistance to acids and makes FRP essentially non-corrosive. Besides, it's also easy to operate and does not involve heavy

*Associate Professor, College of Civil Engineering and Architecture, Guangxi University, Nanning, China; College of Civil Engineering and Architecture, Guilin University of technology, Guilin 541000, China (E-mail: shuangchen81@163.com)
**Professor, Hezhou University, Hezhou 542800, China (E-mail: hb@glut.edu.cn)
***Professor, College of Civil Engineering and Architecture, Guilin University of technology, Guilin 541000, China (Corresponding Author, E-mail: tianmu77@163.com)
****Lecturer, College of Civil Engineering and Architecture, Guilin University of technology, Guilin 541000, China (E-mail: zhangjse@qq.com)

equipment on the construction site. Substantial studies have shown that the reinforcement of corrosion RC beams and slabs with externally bonded FRP sheets are efficient in restoring the flexural and shear strength of test specimens (Chin *et al*., 2015). Furthermore, some studies have revealed that the FRP sheets wrapped around RC members could be considered as a barrier against the water, air and chloridion from permeating into the concrete (Al-Rousan and Issa, 2017). Therefore, the corrosion process could be delayed enormously. However, most of the researches have concentrated on the corrosion of longitudinal reinforcing steel; few have involved the corrosion of stirrups or considered the lose efficacy of stirrups (Al-Saidy *et al*., 2016; El-Maaddawy and Chekfeh, 2013; Li *et al*., 2016).

In this work, an experiment of 12 corroded RC beams was carried out and the corrosion rate was varied from 0% to 18% which represented the mass lose in reinforcement steel in the tension side. The main objective is to explore the impact of lose efficacy of stirrups on the arch effects for RC beams with different corrosion rate, and the effectiveness of CFRP in reinforcing the arch behavior of structural has also been considered.

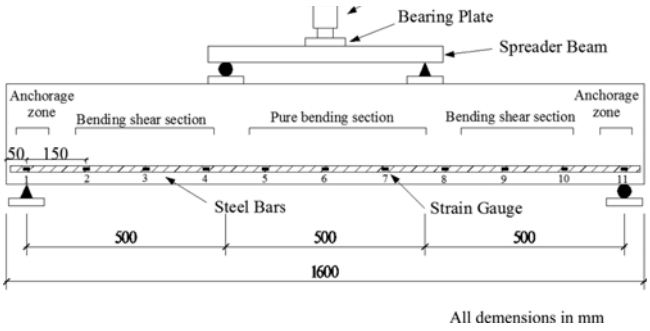

Fig. 1. Schematic Diagram of Loading Device and Steel Strain Gauge Number

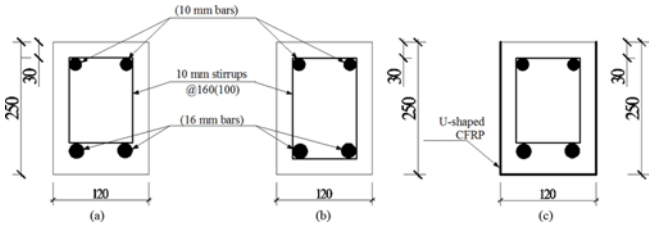

Fig. 2. Schematic Diagram of Cross-section for Test Beams: (a) Group A, (b) Group B, (b) Group

2. Test Design

2.1 Construction Materials

The hot-rolled ribbed reinforcing bars of tension side were 16 mm in diameter with measured average yield strength of 410 MPa; the hanger bars were the same with longitudinal bars but were 10 mm in diameter; the measured yield strength of the 6 mm diameter plain stirrups was 340 MPa.

The concrete was cast with ordinary Portland cement, river sand with the fineness modulus of 2.5, coarse aggregate with a maximum grain size of 20 mm and tap water. The mix proportion of the concrete is shown in Table 1.

Unidirectional carbon fiber sheets with a thickness of 0.167 mm and tensile strength of 3000 MPa were used for the bottom longitudinal reinforcing sheets and the U-shaped strips. The epoxy was used to bond the CFRP to the concrete surface.

2.2 Specimen Design

Twelve rectangular reinforced concrete beams of 1600 mm long, 120 mm wide and 250 mm deep were cast. The designed strength grade of concrete was C30 and the thickness of concrete cover was 30 mm. Using the strain gauges to measure the strain of reinforcements, the position and number of the strain gauges are shown in Fig. 1. All the test beams were divided into three groups as summarized in Table 2.

In order to simulate the situation that the stirrups were seriously corroded, the longitudinal tension reinforcements of beams in Group A were not wrapped by the stirrups, but only fixed by steel wires as shown in Fig. 2. Beams of Group B were common control beams without CFRP reinforcement. Beams of Group C were corroded and then repaired by applying longitudinal CFRP sheets at the bottom and additional U-shaped CFRP sheets around the cross-section as shown in Fig. 3 (Barros *et al*., 2017). Besides, the anti-rust processing of stirrup was operated on test beams in Group B.

Table 1. The Mixture of Concrete

Strength grade of concrete	Coarse aggregate (kg/m^3)	Sand (kg/m^3)	Cement (kg/m^3)	Sand coarse aggregate ratio (%)	5% NaCl solution (kg/m^3)	Water cement ratio
C30	1198	648	380	35	185	0.49

Table 2. Specimen Grouping and Design Points

Corrosion ratio (corrosion time)	Group A (To simulate the stirrups has no restriction on Longitudinal reinforcement)	Group B (Common stirrups with anti-corrosive treatment)	Group C (Reinforced by CFRP)
0% (0)	A0	B0	C0
6% (21.9d)	A6	B6	C6
12% (43.9d)	A12	B12	C12
18% (65.7d)	A18	B18	C18

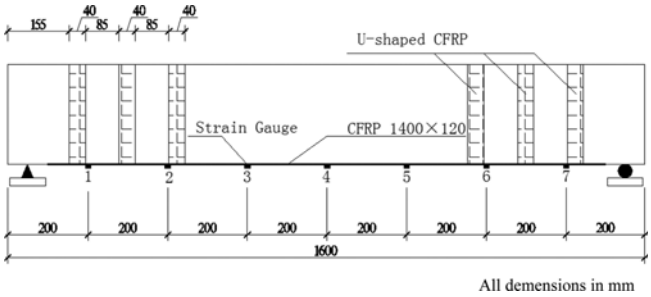

Fig. 3. Carbon Fiber Sheet Reinforcement Scheme and Strain Gauge Arrangement and Numbering

Four RC beams in each group, as in the case of Group A, named A0, A6, A12 and A18, were subjected to accelerated corrosion with theoretical 0%, 6%, 12% and 18% (mass loss in reinforcement) respectively.

After casting, the beams were cured in a natural indoor environment at a temperature of 23±3°C and 95% relative humidity for 28d.

2.3 Accelerated Corrosion Progress and Load Setup

To ensure their electrical conductivity, before the specimens were corroded, they had been immersed in the solution of 5% sodium chloride for 3 days. The corrosion time was calculated using Faraday's law expressed by Eq. (1) as follow (Zeng *et al.*, 2009):

$$t = \frac{mZF}{MI} \tag{1}$$

Where, F = Faraday's constant
I = Corrosion current (200 mA/cm^2 in this test)
m = Mass loss (g)
M = Molar mass of iron (56 g/mol)
Z = Valence of the reacting electrode for the material (2 in this test)

The calculated corrosion time for each group is shown in Table 2

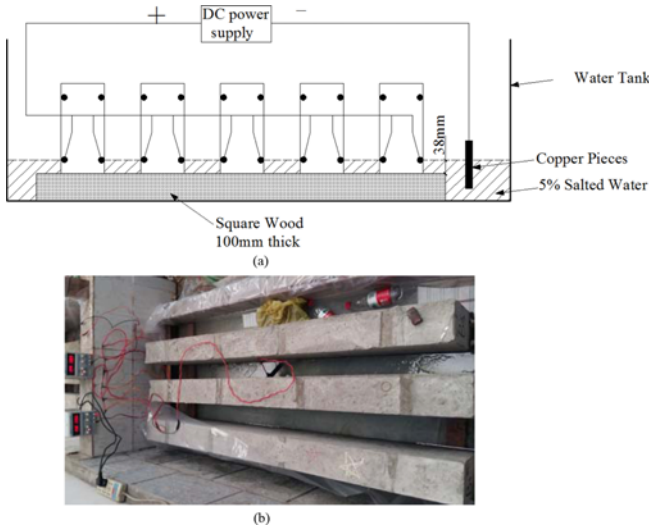

Fig. 4. Schematic and Photos of Accelerated Corrosion Setup: (a) Schematic of Accelerated Corrosion Setup, (b) Beams under Corrosion

and the schematic along with the photos of accelerated corrosion setup is shown in Fig. 4 (Azam and Soudki, 2012; Davis *et al.*, 2016).

A 250 kN hydraulic actuator and spreader steel beam were used to apply the load (3 kN at each level) to the specimens until the specimens were damaged (concrete crush or CFRP pulling apart) (Fig. 2). The strain gauge was used to measure the side strain of concrete, meanwhile, three dial indicators was used to measure the deflections at mid-span and both ends of the test beams.

3. Test Results and Discussion

The ultimate loads, mid-span deflections and the failure modes of all test beams are summarized in Table 3.

3.1 Effect of Stirrups

The load versus mid-span deflections curves of Group A and

Table 3. Summary of Test Results for Group A and B C

Test beam	Ultimate load/(KN)	Ultimate deflection/mm	Mode of failure
A0	114	14.34	shear failure, concrete crush in compression zone
A6	78	9.12	shear failure
A12	66	7.50	shear failure
A18	54	7.10	anchorages failure
B0	120	14.94	shear failure, concrete crush in compression zone
B6	99	10.69	shear failure, concrete crush in compression zone
B12	90	9.44	shear failure
B18	72	8.02	anchorages failure
C0	132	13.53	shear failure, concrete crush in compression zone
C6	120	10.34	shear failure, concrete crush in compression zone
C12	117	15.12	shear failure, concrete crush in compression zone
C18	102	11.21	anchorages failure, U-shaped CFRP peel off

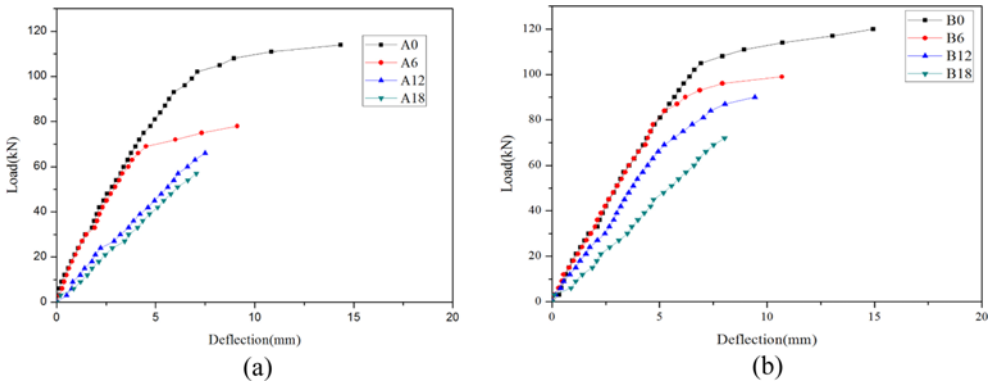

Fig. 5. Effect of Stirrups: (a) Group A Beams, (b) Group B Beams

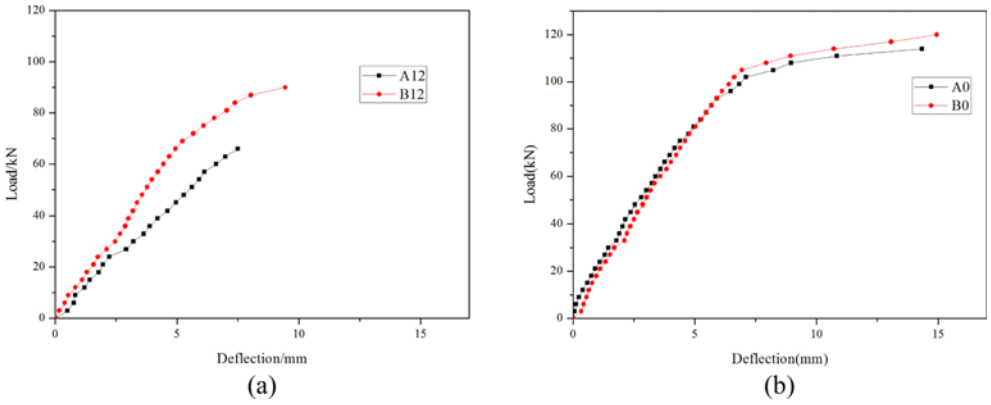

Fig. 6. Effect of Corrosion: (a) Beams A12 and B12, (b) Beams A0 and B0

Group B are shown in Fig. 5. In general, the curves of Group B reflects the adverse effect of corrosion of longitudinal steel bars on the stress state of test beam, and the comparison between Group A and Group B reflects the effect of corrosion of stirrups.

It is observed that the load ~ deflection curves of beam beam A0, A6, B0 and B6 were similar: the increasing speed of deflection suddenly accelerated once the test loads reached the turning points. Compared with the failure processes of the specimens, these turning points actually represented the yield points of the tensile reinforcements, and the failure modes of these 4 test beams were ductile. This showed that although the corrosion of stirrups had an effect on the stress, when the corrosion rate was relatively low, it would not fundamentally change the stress state of the beam.

On the other hand, the load ~ deflection curves of beam A12, A18, B12 and B18 were similar: they all didn't have obvious turning points. It was also observed that the vertical cracks located in pure bending section of A12 and A18 developed slowly, while the diagonal cracks in bending shear section developed rapidly, and the diagonal cracks were almost as wide as the longitudinal main crack at the bottom of the beams. Accordingly, beam A12, A18, B12 and B18 all failed in a brittle manner by crushing of concrete after the steel bars had yielded. However, there was no significant difference between stress modes of beam A18 and B18, which meant that when the corrosion rate was extremely high, the bond stress between steel bars and concrete almost completely disappeared, so that the stirrups had little effect on the bending state of the beams.

The ultimate loads were 57.5, 62.2,75.4 and 114.5 kN for beams A18, A12, A6 and A0, respectively. This indicated a reduction in load of 52.6%, 42.1% and 31.5% in beams A18, A12 and A6 relative to the non-corroded beam A0. Compared to Group A, the load reduction rates were 40%, 25% and 17.5% in beams B18, B12 and B6 relative to beam B0. It's noted that the reductions of ultimate loads for Group A were greater than the normal beams in Group B because of the failure of stirrups.

To make it clear, the comparisons of load-deflection behavior of A0 with B0 and A12 with B12 are shown in Fig. 6.

The control beam A0 and B0 both failed in a ductile manner and the discrepancies of ultimate load and deflection between them were small. However, the situation was quite different when the beams were corroded. The failure load of beam A12 was 66 kN, which decreased by 26.7% compared to the ultimate load of beam B12. The ultimate deflection of beam A12 was 7.5 mm, which was only 79.4% of beam B12. The beam B12 failed in a ductile manner, while the beam A12 showed a brittle behavior. From the above comparison, it can be concluded that the corrosion of stirrups results in the degradation of the bearing

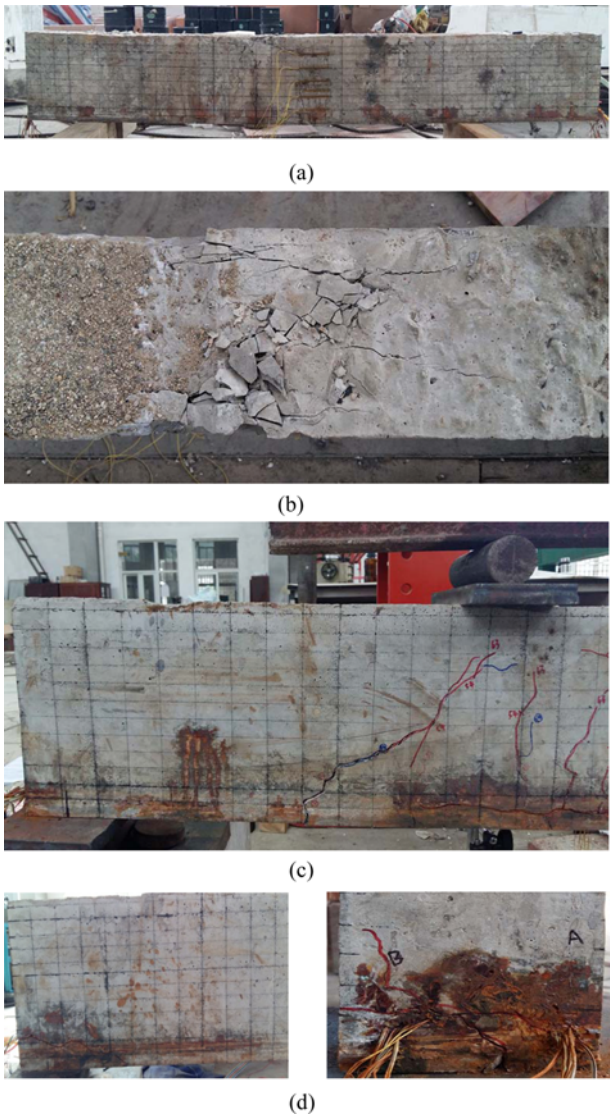

Fig. 7. Photos of Different Failure Modes: (a) Concrete Crushing of Beam A0: (b) Vertical View of Beam A0, (c) Sheer Failure of Beam A12, (d) Bond Failure of Beam A18

capacity and stiffness of all beams due to the loss of bond stress between rebar and concrete. Meanwhile, an early shearing failure in bending-shear section of beam A12 occurred because of the lacking of shear capacity caused by the stirrups failure.

During the test it is observed that vertical cracks in pure bending section of the beam A12 developed slowly, but the diagonal cracks of bending-shear section developed relatively fast. The diagonal cracks almost developed throughout loading point to the bottom of the beam, and the main diagonal crack was wider than the vertical crack. The photos of cracks are shown in Fig. 7.

3.2 Stress of Longitudinal Reinforcement Analysis

Eleven strain gauges evenly were distributed on the longitudinal reinforcement of each test beam (shown in Fig. 1), and five of them were chosen to draw the load-strain curves of test beams, as shown in Fig. 8. Strain gauges (No. 1 ~ 4) were from the bending-shear zone and strain gauge No. 5 located in the pure bending zone.

The figure shows that when the load was small, the strain and the load had a linear relationship on all five positions. The test beams did not crack and the effect of the stirrups was not shown, so the differences between Group A and Group B were unapparent.

With the increase of the load, the first main crack appeared in the pure bending area and there were many tiny vertical cracks beside it; the concrete in the tension zone was out of work, so the tensile stress was assumed by the reinforcements only. Take the No. 5 strain gauge of beam B0 as an example, when the load reached 22 kN the main bending crack appeared, so the strain increased sharply.

Along with the increase of the load, the curves of the strain gauge 1 and 2 located on the anchorage area also increased suddenly. There are two reasons for the sudden increase: first, the diagonal cracks had led to this area where the concrete also pulled out of work, so the stress of the rebar increased suddenly; second, the bond stresses of highly corroded test beams seriously lost, so more and more slight bond failures appeared in the anchorage area when the load grew larger.

After the steel bars were yielded, the strain of the rebar increased rapidly till the ultimate bearing load of the beam was reached, even if the load increased slightly. Due to the existence of longitudinal cracks, the tensile steel bars had been sliding, which resulted in the rapid increase of the strain at both beam ends. It's indicated that the stress of the reinforcement transferred from the mid-span to the anchor ends, and was mainly assumed by the intact anchor ends.

The results showed that the transfer efficiency of beams in Group A was more than that of beams in Group B under the same corrosion rate. Besides, the greater the corrosion rate was, the more obvious the transfer effect was. This indicated that the existence of stirrups played an important role in the stress redistribution of the longitudinal reinforcement.

3.3 The Calculation of Arch Effect

To study the bearing mechanism of the RC beams during load process under different corrosion rate and the stirrup failure behavior (Wang *et al*., 2017), the reinforced stress-strain model used in this paper is shown in Fig. 9. When the corrosion rate was low and the yield platform existed, the model A was employed. When the corrosion rate was high, the rebar hardening strain ε_{shc} degenerated to yield strain ε_{syc} and the yield platform of steel bar disappeared, the model B was employed.

Where, f_{uc} = Nominal yield strength of uncorroded steel
f_{u0} = Ultimate strength of uncorroded steel
f_{yc} = Nominal yield strength of corroded steel
f_{y0} = Yield strength of uncorroded steel
ε_{shc} = Strain hardening of corroded steel
ε_{suc} = Ultimate strain of corroded steel
ε_{syc} = Yield strain of steel
η_s = Corrosion rate of steel

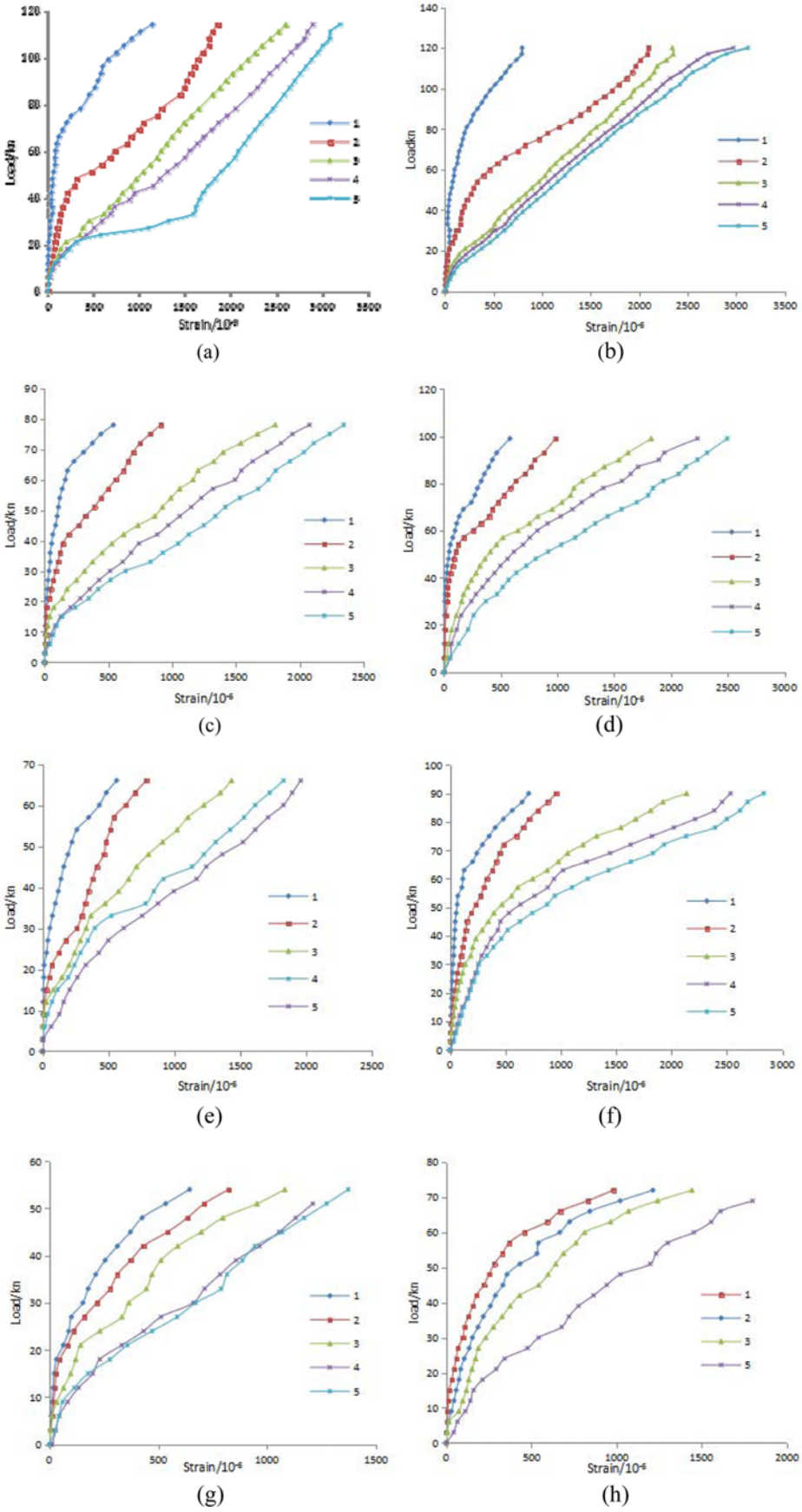

Fig. 8. Load-strain Curves of Test Beams: (a) B0, (b) A0, (c) B6, (d) A6, (e) B12, (f) A12, (g) B18, (h) A18

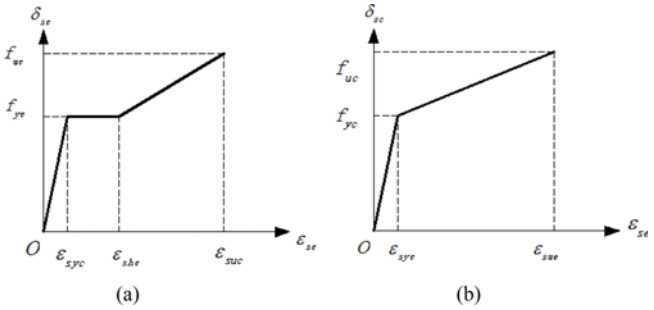

Fig. 9. Stress-strain Model of Reinforced Bar: (a) Model A, (b) Model B

Table 4. Yield Strength, Ultimate Strength and Effective Area of Steel with Different Corrosion Rates

Corrosion rate	f_{yc} (N/mm^2)	f_{uc} (N/mm$_2$)	A_s (mm)
0%	400	540	352.11
6%	349.6	488.16	330.98
12%	299.3	426.60	309.85
18%	248.8	365.04	253.52

The formulas 2 and 3 are used for the calculation of f_{yc} and f_{uc}, and the result are shown in Table 4 (Wu and Yuan, 2008).

$$f_{yc} = f_{y0}(1 - 0.021\,\eta_s) \tag{2}$$

$$f_{uc} = f_{u0}(1.018 - 0.019\,\eta_s) \tag{3}$$

The tension force of corroded steel bars are calculated as follow:

$$F_{yc} = f_{yc}.A_S \tag{4}$$

$$F_{uc} = f_{uc}.A_s \tag{5}$$

The thrust angle of arch effect is calculated as formula (6)?

$$\tan\theta = (h_0 - \frac{x}{2}) / l \tag{6}$$

Where, h_0 = Effective section height
l = Length of bending-shear section (500 mm here)
x = ξh_0 (ξ = 0.518 here)

Then the thrust force of arch effect can be calculated as formula (7) and the diagram of the thrust force is shown in Fig. 10.

$$T = F/\cos\theta \tag{7}$$

The test result and calculation of specimens of different corrosion rate are shown in Table 5.

In general, the arch effects were more obvious with the increase of corrosion rate both in Group A and Group B. However, the arch effects of beams in Group A were greater than that of group B under a same corrosion rate.

The decrease of bond stress between steel bars and concrete was caused by the corrosion. During the loading process, the residual adhesion was damaged as the load increased gradually, and the bond stress almost completely vanished in the position where the serious corrosion took place, which made the stress of

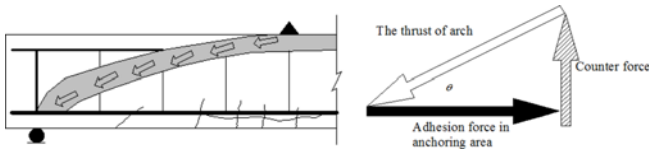

Fig. 10. Schematic Diagram of Arch Thrust

Table 5. Arch Effect of Test Beams

Specimen	Thrust angle	P_U (KN)	F_{uc} (KN)	T_{cu} (KN)	T_{cu}/P_u (%)
A6	17.44°	78	35.81	37.53	48.1
B6		99	38.46	40.31	40.7
A12		66	38.41	40.26	61.2
B12		90	47.32	49.61	55.1
A18		57	32.68	34.26	60.1
B18		72	49.75	52.15	72.43
P_U = Ultimate load					

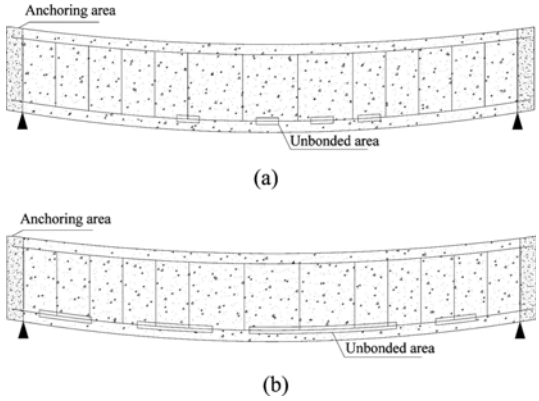

Fig. 11. Schematic Diagram of Loss of Cohesive Force: (a) Early Loading Stage, (b) Late Loading Stage

rebar homogenized. Due to the unevenness of the corrosion, the bond failure was distributed in different positions of the steel bars, which could be regarded approximately as a number of tie rods. As the load level increased, more and more tension zones of the concrete were out of work. Therefore as the number of the tie rods were reduced, the overall arch effects of test beams were more obvious, as shown in Fig. 11.

The conversion rates of arch effect for beam A18 and B18 were 60.1% and 72.43%, respectively. This is because the diagonal cracks of beam A18 without stirrups developed relatively fast than that of beam B18. When the load reached 57 kN, the diagonal cracks of beam A18 crossed over the longitudinal main crack located at the beam bottom. Then, beam A18 lost its bearing capacity due to an anchor failure at a relative early stage.

The arch tension propositions of other beams in Group A were higher than that of Group B (except A18 and B18). Although the width and length of diagonal cracks in Group A were greater than that in Group B under the same corrosion rate when the load level was relative high, the diagonal cracks didn't connect with the longitudinal main crack through the bottom of test beams. So

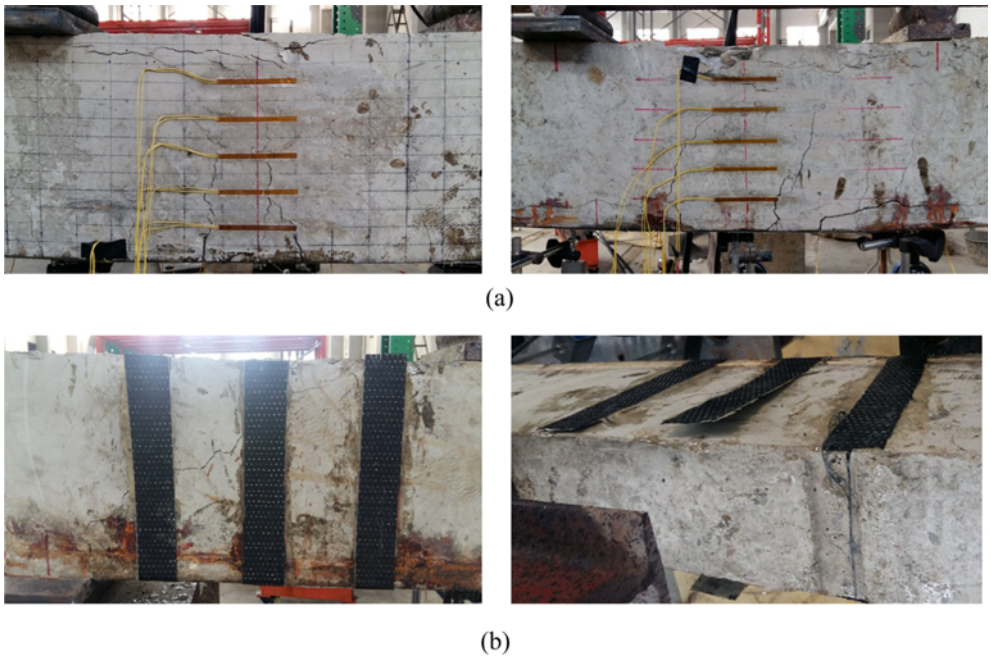

Fig. 12. Photos of Different Failure Modes: (a) Concrete Crushing of Beam C6, (b) U-shape CFRP Peeling Away of Beam C18

the tensile stress in both anchor ends of beams in Group A was still strong enough to act as the arch tensile (Dong *et al*., 2011; Feng *et al*., 2016), because the anchorage failure had not occurred in both ends. In conclusion, the adhesion on the beam anchorage is the basis for arch effect.

3.4 The Effect of CFRP

The secondary reinforcement tests were carried on test beams of Group C. When the load reached 30 kN, the loading progresses were holding still and the CFRP were bonded to the test beams. The second loading process continued after an interval of 48H, in order to make sure that the adhesive epoxy between CFRP and concrete was fully cured.

The ultimate load, mid-span deflection and the failure mode of Group C are summarized in Table 3 and the photos of different failure modes are shown in Fig. 12.

The ultimate load of beam C0, C6, C12, C18 increased 15.8%, 53.8%, 77.3%, 78.9% compared with beam A0, A6, A12, A18. It can be concluded that the ultimate bearing capacities and stiffness of the beams of Group C were improved a lot under the same corrosion rate compared with beams of Group A because of two reasons: first, the longitudinal CFRP was involved in tension, which compensated for the loss of tensile capacity due to the corrosion of the steel bars; second, the U-shaped CFRP could constrain the development of diagonal cracks effectively, by enhancing the shear force between the diagonal cracks. Moreover, it can be observed that the strengthening effect of CFRP was obviously improved with the increase of corrosion rate.

However, the corrosion expansion cracks had a great influence on strengthening effect. For example, the expansion cracks of beam C6 were not obvious, and the beam was broken with the crush of concrete. As a comparison, the corrosion expansion cracks of beam C18 had developed extremely obvious before loading, and the cracks had been developing toward the anchor ends as the load increased. Finally beam C18 failed because of the anchor failure, and the U-shaped CFRP were also peeled off because of the lack of shearing force.

4. Conclusions

This study presented test results and discussions on the structural behavior of corroded RC beams. Based on the test results, the following conclusions are drawn:

1. The corrosion of stirrups affects the components' stress state from two aspects: the first aspect is the decrease of shear capacity caused by the bond failure between concrete and stirrups. The second aspect is the reduction of the restriction on the slip of longitudinal reinforcement. The Influence was reflected in the differences of ultimate loads, ultimate deflections, crack developments and failure modes between experimental beams of Group A and Group B. These differences were more obvious as the corrosion rate increased.
2. The bond stress between steel bars and concrete were seriously degenerated due to the corrosion of steel bars. The bond stress transferred from the mid-span of the beams to the anchor ends during the loading process, and the mechanical mode of experimental beams tended to act like an arch. The greater the corrosion rate, the more obvious the arch effect.
3. The longitudinal reinforcement was better bonded with the concrete because of the existence of stirrups. And the mechanical resistance between the longitudinal reinforcement and the stirrups prevented the longitudinal bars from slipping. Therefore,

the arch effects of component with corroded stirrups were greater than that of the normal components.

4. During the secondary reinforcement test, the ultimate bearing capacity of corroded beams reinforced by CFRP was increased by an average of 56.5%, much higher than 15.8% of the non corroded beam. So, it's effective to use CFRP to reinforce beams with corroded stirrups. However, the longitudinal cracks of the test beam were fully developed when the corrosion rate was particularly high, which leaded to the reduction of the reinforcement effect of CFRP.

Acknowledgements

This paper is supported by the National Natural Science Foundation of China (51268009), the foundation of High Level Innovation Team of Guangxi Province, and Research Project of University in Guangxi. (201106LX028), the views expressed are authors' alone.

References

Al-Hammoud, R., Soudki, K., and Topper, T. H. (2010). "Bond analysis of corroded reinforced concrete beams under monotonic and fatigue loads." *Cement and Concrete Composites*, Vol. 32, No. 3, pp. 194-203, DOI: 10.1016/j.cemconcomp.2009.12.001.

Al-Rousan, R. Z. and Issa, M. A. (2017). "Flexural behavior of RC beams externally strengthened with CFRP composites exposed to severe environment conditions." *KSCE Journal of Civil Engineering*, Vol. 21, No. 6, pp. 2300-2309, DOI: 10.1007/s12205-016-0570-x.

Al-Saidy, A. H., Al-Harthy, A. S., Al-Jabri, K. S., Abdul-Halim, M., and Al-Shidi, N. M. (2010). "Structural performance of corroded RC beams repaired with CFRP sheets." *Composite Structures*, Vol. 92, No. 8, pp. 1931-1938, DOI: 10/1016/j.compstruct.2010.01.001.

Al-Saidy, A. H., Saadatmanesh, H., and El-Gamal S. (2016). "Structural behavior of corroded RC beams with/without stirrups repaired with CFRP sheets." *Materials and Structures*, Vol. 49, No. 9, pp 3733-3747, DOI:10.1617/s11527-015-0751-y.

Azam, R. and Soudki, K. (2012). "Structural performance of shear-critical RC deep beams with corroded longitudinal steel reinforcement." *Cement and Concrete Composites*, Vol. 34, No. 8, pp. 946-957, DOI: 10.1016/j.cemconcomp.2012.05.003.

Badawi, M. and Soudki, K. (2010). "CFRP Repair of RC beams with shear-span and full-span corrosions." *Journal of Composites for Construction*, Vol. 14, No. 3, pp. 323-335, DOI: 10.1061/(ASCE) CC.1943-5614.0000065.

Barros, A. O., Rezazadeh, M., and Laranjeira, P. S. (2017). "Simultaneous flexural and punching strengthening of RC slabs according to a new hybrid technique using U-shape CFRP laminates." *Composite Structures*, Vol. 159, pp. 600-614, DOI: 10.1016/j.compstruct.2016.10.009.

Chin, S. C., Shafiq, N., and Nuruddin, M. F. (2015). "FRP as strengthening material for Reinforced Concrete beams with openings - A review." *KSCE Journal of Civil Engineering*, Vol. 19, No. 1, pp. 213-219, DOI: 10.1007/s12205-011-0162-8.

Coronelli, D. and Gambarova, P. (2004). "Structural assessment of corroded reinforced concrete beams: Modeling guidelines." *Journal of Structural Engineering*, Vol. 130, No. 8, pp. 1214-1224, DOI: 10.1061/(ASCE)0733-9445(2004)130:8(1214).

Davis, M., Hoult, N. A., and Scott, A. (2016). "Distributed strain sensing to determine the impact of corrosion on bond performance in reinforced concrete." *Construction and Building Materials*, Vol. 114, pp. 481-491, DOI: 10.1016/j.conbuildmat.2016.03.205.

Dong, W., Murakami, Y., Oshita, H., Suzuki, S., and Tsutsumi, T. (2011). "Influence of both stirrup spacing and anchorage performance on residual strength of corroded RC beams." *Journal of Advanced Concrete Technology*, Vol. 9, No. 3, pp. 261-275, DOI: 10.3151/jact.9.261.

El-Maaddawy, T. and Chekfeh, Y. (2013). "Shear strengthening of T-beams with corroded stirrups using composites." *ACI Structural Journal,* Vol. 110, No. 5, pp. 779-789.

Feng, Q., Visintin, P., and Oehlers, D. J. (2016). " Deterioration of bond-slip due to corrosion of steel reinforcement in reinforced concrete." *Magazine of Concrete Research*, Vol. 68, No. 5, pp. 768-781, DOI: 10.1680/jmacr.15.00217.

Kreit, A., Al-Mahmoud, F., and Castel A. (2014). "Repairing corroded RC beam with near-surface mounted CFRP rods." *Materials and Structures*, Vol. 44, No. 5, pp. 1205-1217, DOI: 10.1617/s11527-008-9460-0.

Li, H., Wu, J., and Wang, Z. (2016). "Shear performance of reinforced concrete beams with corroded stirrups strengthened with carbon fiber-reinforced polymer." *ACI Structural Journal*, Vol. 113, No. 1, pp. 51-61.

Schnerch, D., Dawood, M., Rizkalla, S., Sumner, E., and Stanford, K. (2006). "Bond behavior of CFRP strengthened steel structures." *Advances in Structural Engineering*, Vol. 9, No. 6, pp. 805-817, DOI: 10.1260/136943306779369464.

Soudki, K. and Sherwood, T. (2003). "Bond behavior of corroded steel reinforcement in concrete wrapped with carbon fiber reinforced polymer sheets." *Journal of Materials in Civil Engineering*, Vol. 15, No. 4, pp. 358-370, DOI: 10.1061/(ASCE)0899-1561(2003)15:4(358).

Wang, L., Yi, J., Xia, H., and Fan, L. (2016). " Experimental study of a pull-out test of corroded steel and concrete using the acoustic emission monitoring method." *Construction and Building Materials*, Vol. 122, pp. 163-170, DOI: 10.1016/j.conbuildmat.2016.06.046.

Wang, L., Zhang, X., and Zhong, L. H. (2017). "Analysis of mechanical properties and arch effect of corroded reinforced concrete Beams." *Journal of Huaqiao University*, Vol. 38, No. 1, pp. 24-30. (in Chinese).

Wu, Q. and Yuan, Y. S. (2008). "Experimental study on the deterioration of mechanical properties of corroded steel bars." *China Civil Engineering Journal*, Vol. 41, No. 12, pp. 42-47. (in Chinese)

Xia, J., Jin, W. L., and Li, L. Y. (2011). "Shear performance of reinforced concrete beams with corroded stirrups in chloride environment." *Corrosion Science*, Vol. 53, No. 5, pp. 1794-1805, DOI: 10.1016/j.corsci.2011.01.058.

Xue, X., Seki, H., and Song, Y. (2014). "Shear behavior of RC beams containing corroded stirrups." *Advances in Structural Engineering*, Vol. 17, No. 2, pp. 165-177, DOI: 10.1260/1369-4332.17.2.165.

Zhou, H. J., Lu, J. L., Xv, X., Dong, B. Q., and Xing, F. (2015). " Effects of stirrup corrosion on bond-slip performance of reinforcing steel in concrete: An experimental study." *Construction and Building Materials*, Vol. 93, pp. 257-266, DOI: 10.1016/j.conbuildmat.2015.05.122.

Zeng, Y. (2014). "Study on degradation of bond properties of corroded reinforced concrete and its influence to the flexural stiffness of beam." PhD Thesis, Chongqin University, CN. (in Chinese)

Zeng, Y. H., Gu, X. L., and Zhang, W.P. (2009). "Accelerated corrosion technique for reinforcement steel bars in concrete." *Structural Engineers*, Vol. 25, No. 1, pp. 101-105. (in Chinese)